The 8th Pacific Rim International Conference on Advanced Materials and Processing

ENGINEERING THIN FILM SEMICONDUCTOR GAS SENSORS TO INCREASE SENSITIVITY AND DECREASE OPERATION TEMPERATURE

John Bell, Tuquabo Tesfamichael

Science and Engineering Faculty, Queensland University of Technology
2 George Street, Brisbane, 4000, QLD Australia

Keywords: Tungsten oxide, iron doping**,** nanostructured thin films, gas sensing

Abstract

Thin film semiconductor gas sensors typically operate at temperatures above 400^{o}C, but lower temperature operation is highly desirable, especially for remote area field sensing as this reduces significantly power consumption. We have investigated a range of sensor materials based on both pure and doped tungsten oxide (mainly focusing on Fe-doping), deposited using both thermal evaporation and electron-beam evaporation, and using a variety of post-deposition annealing. The films show excellent sensitivity at operating temperatures as low as 150^{o}C for detection of NO_2. There is a definite relationship between the sensitivity and the crystallinity and nanostructure obtained through the deposition and heat treatment processes, as well as variations in the conductivity caused both by doping and heat treatment. The ultimate goal of this work is to control the sensing properties, including selectivity to specific gases through the engineering of the electronic properties and the nanostructure of the films.

Introduction

Thin film nanostructured metal oxide sensors hold enormous promise to enable a new generation of gas sensing applications due to their ability to achieve nearly continuous monitoring of gases at a large number of locations. However, most of the nanostructured metal oxide gas sensors that have been investigated to date are not sufficiently sensitive at lower temperatures (<200^{o}C) to be used in most applications. The sensors must thermally be activated at elevated temperatures (>400^{o}C) and this leads to a long-term material stability problem due to diffusion and sintering effects. The high operating temperatures of the sensors also demand higher power consumption [1], which makes them unsuitable for battery operated sensing that would be advantageous in many applications. Lower operating temperature gas sensors (<200^{o}C) would overcome the stability and high power consumption problems occurring in the high temperature sensors.

Semiconducting materials so far investigated for gas sensing include SnO_2, TiO_2, ZnO, In_2O_3, MoO_3 and WO_3 and thsese materials have band-gap energy between 2.6 to 3.3 eV at room temperature. The most common sensing mechanisim of the metal oxide sensors involves the changes in the electrical resistance (conductivity) induced by reactions between the target gas and the film surface. These reactions cause injection or extraction of electrons from the metal oxide, changing the conductivity of the material. Key sensor response parameters characterising the sensing behaviour of the metal oxide sensors are the sensitivity, or sensor response amplitude (S), of the device, the response and recovery times (τ_{RESP} and τ_{REC}). The sensor response amplitude (S) is defined to be a positive quantity and for oxidizing gases (e.g.

NO_2) [2]: $S=(R_{gas}-R_{air})/R_{air}=\Delta R/R$; where R_{gas} and R_{air} are the steady state resistance values achieved within reasonable time (<20 min) during the exposure of the sample to the reference gas (synthetic air) and target gas (NO_2), respectively. For reducing gas such as CO, NH_3 and H_2, $R_{gas} < R_{air}$ and the response of the sensors can be quantified using the conductivity change [2]: $S=(G_{gas}-G_{air})/G_{air}=\Delta G/G$; where $G_{gas} > G_{air}$ are the steady state conductivity values measured within acceptable time (<20 min) during the exposure to the reference and target gases, respectively. The response (τ_{RESP}) and recovery (τ_{REC}) times are important sensor parameters. The τ_{RESP} was determined as the time the sensor resistance (conductance) takes to reach the 90% of its final value, and τ_{REC} as the time the sensor response takes to recover the 70% of its baseline value. Sesnor performance (sensitivity, selectivity, response and recovery times) is highly dependent on the film characteristics (crystallinity, grain size, defect structure, vacancies, porosity, film thickness, film stoichiometry, and surface morphology), and these can be controlled by changing the deposition conditions, post-deposition annealing, and doping.

Thin films of tungsten oxide (WO_3) deposited by PVD techniques are very promising due to the material's inherent electrical conductivity, typically generated by a slight substoichiometry of these types of films, and good sensitivity towards various gases at lower operating temperatures [3-6]. Porous nanostructured materials have a very large surface-to-volume ratio and offer more surface/gas interaction and thereby enhancing the both sensitivity and response time significantly. A previous theoretical study [7] has shown that sensor response can be significantly enhanced if the grain size is smaller than 50 nm. This has been confirmed by previously published work [4, 6]. Sensors made of WO_3 nanotubes have also shown enhanced gas response due to the large surface area presented by the interior of the nanotube assemblies [8]. Metal inclusions are important for the formation of oxygen vacancies and modification of the electronic structure and band gap energy of metal oxides which are critical to gas sensing. Metal doping can also change sensitivity to specific gases thereby increase the response to specific gases [9]. High response and selectivity of Pd-doped WO_3 films to H_2 gas have been reported at working temperature of 200^oC [10]. The response of WO_3 film to NO_2 and NH_3 has been improved when doped with Ag and Pt, respectively [11]. Studies have shown addition of Cu to WO_3 thin film improved the sensor response when exposed to NO_2 [12] whereas addition of Fe increased the response to ozone, CO and ethanol [13]. It has been reported elsewhere that doping of TiO_2 with Fe increases the oxidation activity of the oxide and this has been related to a higher density of oxygen vacancies [14]. Film thickness is another parameter that can have significant effect in optimizing sensor selectivity and sensitivity [15]. From theoretical and experimental studies, the gas sensing properties of tungsten oxide films are strongly dependent on the relationship between film thickness, crystalline size and Debye length of electrons [2]. There are limited reports in the literature on gas sensing of metal oxides in the film thickness range of 100-500 nm [15]. Tungsten oxide thin films obtained by electron beam evaporation and annealed in the temperature range 350-800^oC for 1-3 hours also indicated a highly effective gas sensing to NO_2 [16].

In this paper we present a summary of results from both thermal evaporation and electron-beam evaporation methods used to produce pure and Fe-doped nanostructured tungsten oxide thin films. Films have been evaluated for sensing properties, characterized by the sensitivity and response times, and selectivity towards specific gases, for gas sensing at lower operating temperatures. The gas sensing properties of Fe-doped tungsten oxide films are not well documented in the literature. Since iron has a similar atomic radius (0.64 nm) as W (0.62

nm), it can be introduced as a substitutional impurity in the WO_3 crystal structure to produce crystal distortions, and its influence on physical, chemical, electronic and gas sensing properties can flow on to the sensing properties of the films. Various target gases (H_2, NH_3, NO_2, CO) at different concentrations (2-10,000 ppm) and operating temperatures (150-300^oC) have been investigated. The selected target gas concentrations are within the threshold limit values (TLV) (e.g. 50 ppm for CO, 25 ppm for NH_3, 3 ppm for NO_2, 600 ppm for H_2 [17]). The microstructure, composition, crystallinity and morphology of the films were analyzed using TEM, AFM, Raman and XPS. The effects of these parameters on gas sensing properties have been discussed. Particularly, the influence of film thickness and Fe-doping on the gas sensing behavior of tungsten oxide thin films to oxidizing gas (NO_2) have closely been investigated.

Experimental

Pure (WO_3) and Fe doped (WO_3:Fe) tungsten oxide films were deposited by both e-beam evaporation and thermal evaporation techniques in high vacuum at room temperature. The deposition processes used for both methods are described below.

Electron Beam Evaporation: Pure and iron (10 at%) doped tungsten oxide thin films were produced using electron beam evaporator with dual electron-guns that enable co-evaporation of two materials simultaneously. The films have been deposited on microscopy glass slides (for film chracterisation) and on a 12 mm x 12 mm alumina substrate (for gas sensing). A 10 mm diameter WO_3 pellet (99.9% purity) and 99.95% purity Fe were used as source targets for evaporation. The WO_3 was first baked in an oven at 800 ^oC for 1 hour in vacuum before used for evaporation to remove any moisture in the material. The substrates were placed normal to the evaporation sources at a distance of about 40 cm from the source materials. The WO_3 and Fe materials were placed separately in two copper crucibles that were kept in water-cooled copper hearth of the two electron guns for evaporation. The WO_3 target and Fe were heated by means of an electron beam from tungsten filaments. The chamber was evacuated to a base pressure of about 1.33 x 10^{-7} mbar with an accelerating voltage of about 4 kV. The tungsten oxide film was grown at an average evaporation rate of 6 nm/min whereas the evaporation rate of Fe during co-evaporation with tungsten oxide was adjusted to 0.6 nm/min. The film thickness was monitored using two independent quartz crystal thickness monitors for WO_3 and Fe. Pure and Fe-doped films of various thicknesses (100-500 nm) were produced and in this paper Fe-doped films of 100, 225, 400 and 500 nm thick along with a 300 nm thick pure film have been investigated. Post deposition annealing of all the films at 300^oC for 1 hour in air has been performed. It has been reported previously that annealing of WO_3 film at temperatures below 300^oC did not increase the initial particle size significantly [18].

Thermal Evaporation: Pure and Fe-doped (0.5 at%) WO_3 thin films were deposited on silicon substrate (film characterisation) and silicon substrates with interdigitated Pt electrodes (for gas sensing). The size of the substrate was 8 mm x 8 mm. The electrode fingers have a line width and height of 100 μm and 300 nm, respectively. Powders of tungsten oxide (99.9% purity, grain size 20 μm) and iron (99.9% purity, grain size 100 μm) were used as evaporation sources. A bell jar type PVD unit (Varian Coater with AVT Control System, Australia) was used to deposit the WO_3 thin films. For the purpose of doping, iron was mixed thoroughly with WO_3 and the mixture was evaporated. The substrates were mounted on a substrate holder which was placed at a distance of 38 cm in line of sight from the evaporation source. Deposition was carried out at about 4 x 10^{-5} mbar. Powder was deposited onto the substrates

at a high evapoartion rate of 35 nm/s. A quartz crystal film thickness monitor was used to control the thickness of the films. After the deposition, the films were annealed at 400^{o}C for 2 hours in air to improve the microstructural properties of the films.

Film Characterisation

The as-deposited WO_3 and WO_3:Fe films obtained using both evaporation methods at room temperature indicated a non-crystalline (amorphous) nature. Post deposition annealing of the e-beam films at 300^{o}C for 1 hour in air has induced more ordered bonding structure than the as-deposited film. Figure 1 shows the cross-sectional TEM images of WO_3 and WO_3:Fe annealed films produced by e-beam evaporation. The films appear uniform and their thickness corresponds to the thickness recorded by the quartz crystal thickness monitors during deposition of the films. The electron diffraction patterns of the Fe-doped film shows a continuous diffraction rings and this indicates that annealing of the sample at 300^{o}C has imparted some degree of crystalline characteristic in the nanostructured film. However, the degree of crystallinity of this film appeared to be lower than the pure tungsten oxide film as observed from their electron diffraction patterns. This can be attributed due to the incorporation of Fe in the pure film which may suppress the ordering and crystallization of the film. Co-deposited can induce different structural properties of the tungsten oxide films and can change the oxidation and annealing behavior.

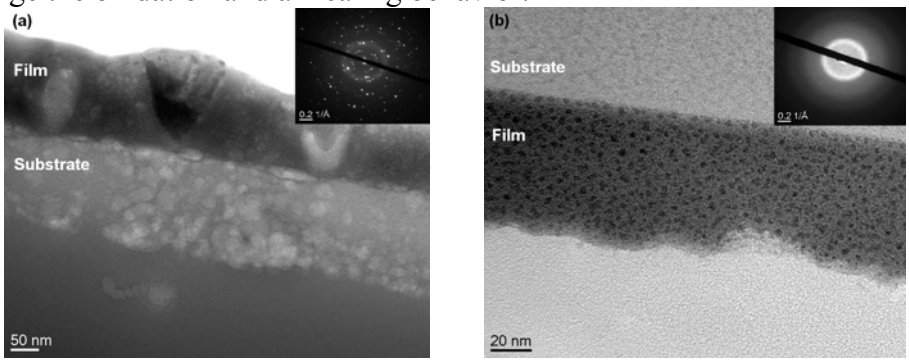

Figure 1. Cross sectional TEM images of e-beam evaporated (a) pure and (b) Fe-doped WO_3 films annealed at 300°C for 1 hour in air. Inset shows the electron diffraction.

The high deposition rate during thermal evaporation at room temperature resulted in highly amorphous films made up of clusters (particles). Figure 2 shows top-view TEM images of thermally evaporated WO_3 and WO_3:Fe films annealed at 400^{o}C for 2 hours in air. Mean grain sizes of about 5 nm and 10 nm were found for the WO_3 and Fe-doped WO_3 films, respectively.

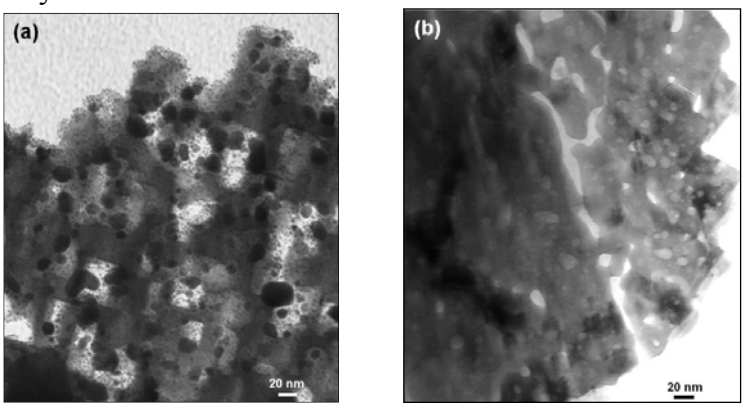

Figure 2. TEM images of thermally evaporated (a) WO_3 and (b) Fe-doped WO_3 films annealed at 400^{o}C for 2 hours in air.

The nucleation, successive grain growth and coalescence during annealing at 400^{o}C transformed these clusters into smaller grains. From literature it has been shown that the crystalline nature of thermally evaporated tungsten oxide films started to occur at substrate temperature of 250^{o}C [23].
Figure 3 shows AFM images of e-beam evaporated WO_3 (Fig. 3a) and WO_3:Fe (Fig. 3b) annealed films with well defined grain boundaries and large porosity. From the AFM analysis, the average grain size of the Fe-doped films (12 nm) was found to be slightly larger than the corresponding values of the pure film (9 nm) as shown in Table 1. This increase in grain size has caused a slight reduction in porosity at the surface of the Fe-doped film. Both films also show very small surface roughness. It has been shown elsewhere that surface roughness decreases sharply when the films were annealed above 200^{o}C [19]. Higher number-grain density was observed in the WO_3:Fe film (355 grains/ μm^2) compared to the number-grain density of in the pure WO_3 film (213 grains/μm^2), and hence a slightly reduced surface area than the pure film. The electron beam evaporation technique has produced nanostructured WO_3 based thin films with significant porosity that is critical in gas sensing applications.

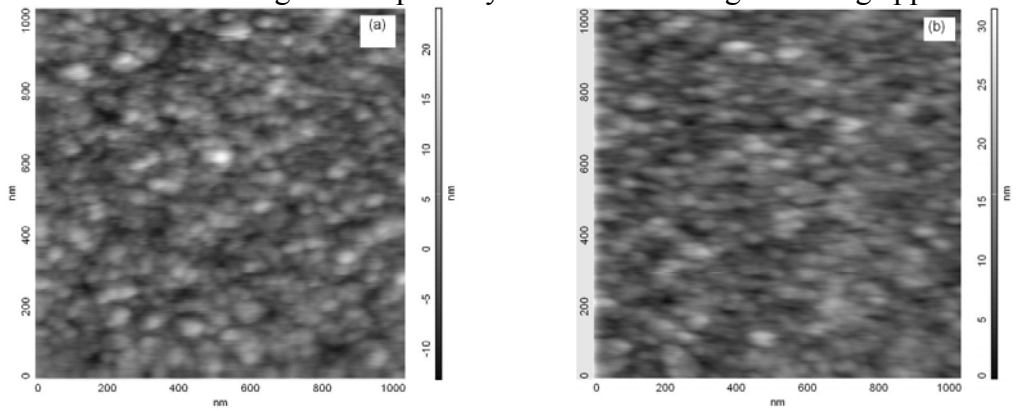

Figure 3 AFM semicontact mode images of e-beam evaporated (a) WO_3 and (b) WO_3:Fe films annealed at 300^{o}C for 1 hour in air.

Table 1. Grain size of e-beam evaporated (EBE) and thermally evaporated (TE) WO_3 and WO_3:Fe films before and after annealing in air.

Material	Grain size (EBE)	Grain size (TE)
As-deposited WO_3	-	13 nm
WO_3 (annealed)	9 nm (300^{o}C)	5 nm (400^{o}C)
As-deposited WO_3:Fe	12 nm	15 nm
WO_3:Fe (annealed)	12 nm (300^{o}C)	10 nm (400^{o}C)

AFM surface topography of the thermally evaporated pure (Fig. 4a) and Fe-doped (Fig. 4b) WO_3 films show a nanostructured surfaces with well defined grains boundaries. The film of the Fe-doped appears to be densely packed compared to pure WO_3 film. Addition of Fe also resulted in a slight increase in roughness compared to the pure film. After annealing at 400^{o}C, however, the grain size decreases. Table 1 shows the grain size information of e-beam and thermal evaporated films before and after annealing in air, obtained by AFM image analysis.

Raman spectroscopy was employed to characterize the chemical and crystalline nature of the WO_3 and WO_3:Fe thin films. Figure 5 shows Raman spectra of both e-beam evaporated (Fig.

5a) and thermal evaporated (Fig. 5b) pure and Fe-doped WO_3 films. As shown in the figure, two typical broad Raman bands in the range of 200-500 cm^{-1} and 550-1050 cm^{-1} can be observed. The first band (200-500 cm^{-1}) is associated to O–W–O bending modes, whereas the second band is related to W–O stretching modes. The bands of the as-deposited films exhibit

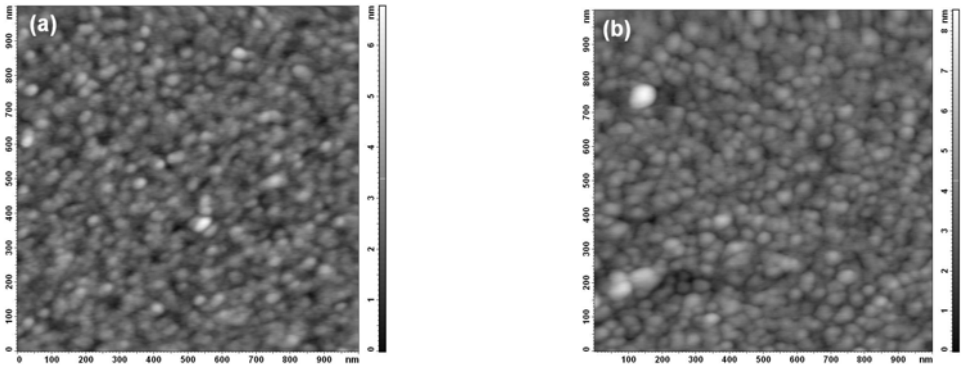

Figure 4. AFM semicontact mode images of thermally evaporated as-deposited (a) WO_3 and (b) Fe-doped WO_3 films.

weak peaks which features amorphous characteristic of the films. Raman peaks of the pure film positions at about 954 cm^{-1} and 779 cm^{-1} are usually assigned in the literature to the stretching frequency modes of bridging oxygen W=O and O-W-O, respectively [11]. Amorphous and nanostructured tungsten oxide films are usually composed of O–W–O mode, reminding the WO_6 octahedral of the bulk crystal, with terminal W=O on their boundaries [20]. The annealed films show some degree of crystallinity with broadening of the peaks which is also confirmed by TEM. From AFM (Table 1), the average grain sizes of the Fe-doped films are found to be slightly larger than the pure films. This can be well explained from the ratio of integrated Raman intensities of W=O band to that of O–W–O band [21] in Figure 5.

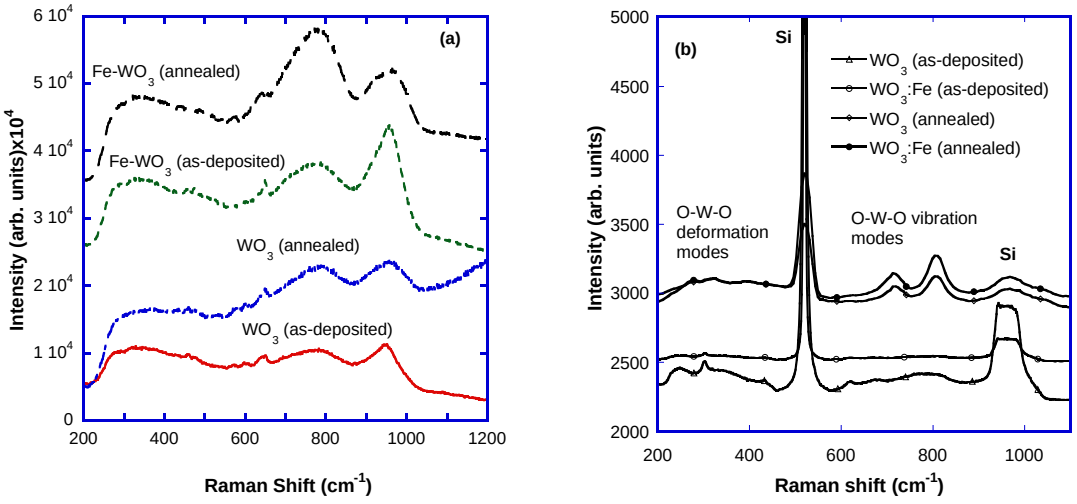

Figure 5. Raman spectra of WO_3 and WO_3:Fe films (a) e-beam evaporated films before and after annealing at 300°C for 1 hour in air and (b) thermally evaporated films before and after annealing at 400°C for 2 hours in air.

The e-beam evaporated films were found to be amorphous to XRD. However, grazing incidence XRD analysis of the thermally evaporated films has shown that the lattice parameters of Fe-doped WO_3 film are slightly smaller than WO_3 film. The GIXRD and Raman analysis indicate that addition of Fe to WO_3 film resulted in slight distortion of the

lattice structure (shortening of O-W-O bonds), owing to the slightly larger ionic radius of Fe^{3+} over W^{6+}, consequently resulting in a slight shift in XRD as well as Raman peaks. However, the octahedral orientation of WO_3 has been retained after doping with Fe, indicating that the preferred oxidation state of Fe is Fe^{3+}. This is evident from similar XRD patterns of 400°C annealed WO_3 and Fe-doped WO_3 films and no evidence of any Raman peaks associated with Fe in 400°C annealed Fe-doped WO_3 film. XRD and Raman analysis have revealed that Fe is incorporated in the host WO_3 matrix as a substitutional impurity rather than as a catalyst on the film surface. Fe-doping and subsequent annealing at 400°C has resulted in smaller cell parameters and shortening of O-W-O bonds.

High resolution XPS spectra of the pure and Fe-doped tungsten oxide films developed by e-beam evaporation and thermal evaporation have been analyzed. From the high resolution spectra the peak positions of W 4f, O 1s, and Fe 2p have been determined as shown in Table 2. The values were determined by calibration and fixing the C (1s) line to binding energy of 284.8 eV. The binding energies corresponding to the various oxidation states vary noticeably in the literature, depending on the energy reference [22, 23]. The core level of the pure tungsten oxide film (both as-deposited and annealed) shows the characteristics of stoichiometric WO_3. The results obtained in this paper are similar to the corresponding XPS spectra of WO_3 films reported elsewhere and the results reveal the presence of W^{6+} [22, 24]. Upon Fe-doping, the peak was shifted towards lower binding energy, indicating the presence of higher number of oxygen vacancies in the doped film, which is beneficial from gas sensing perspectives. The O 1s peak of the pure film is associated with the oxygen bound to tungsten atoms. This peak is shifted to lower binding energy after Fe-doping which confirms the presence of oxygen vacancies in the doped film. The presence of Fe on the e-beam evaporated film has been confirmed from the XPS measurements. The Fe 2p spectrum of the e-beam contained a broader peak of iron oxides (centered at 712 eV) which resulted from Fe^{+3} species [13]. However, in comparison to the pure tungsten oxide film, crystallization of the Fe-doped films during annealing was suppressed up to 300°C. It is to be noted that no Fe-peak was observed from the thermally evaporated films which may be due to the segregation of Fe towards the film/substrate interface. XPS analysis, however, revealed that the annealed films contain high number of oxygen vacancies which is highly beneficial for gas sensing.

Table 2 XPS peak positions of W 4f, O 1s and Fe 2p of both e-beam evaporated (EBE) and thermal evaporated (TE) WO_3 and WO_3:Fe films.

	Peak Position BE (eV)							
	WO_3		annealed WO_3		WO_3:Fe		annealed WO_3:Fe	
	EBE	TE	EBE	TE	EBE	TE	EBE	TE
W $4f_{7/2}$	36.4	35.74	36.2	35.44	36.1	35.8	35.9	35.6
O 1s	531.2	530.7	531.0	530.4	531.0	530.7	530.8	530.4
Fe 2p	-	-	-	-	-	-	712	-

Gas Sensing Measurements

Gas sensing tests have been carried out by flow through method in a thermostatic sealed chamber with controlled temperature and humidity. The sensing properties of each sensor as a function of operating temperature, type of gas and concentrations have been performed. Four different types of target gases (CO, H_2, NH_3, NO_2) with concentrations ranging between 2-10,000 ppm were tested at various operating temperatures (100-300°C). All measurements

have been carried out using gas flow of 200 sccm in 0% RH at room temperature or 300 sccm in 30% RH at 20°C.

Sensing Characteristics to NO_2: Figure 7 shows dynamic response of e-beam evaporated WO_3 (300 nm thick) and WO_3:Fe (225 nm thick) films to difference concentrations (0.5-5 ppm) of NO_2. According to the figure, doping with Fe decreases the material resistance by a factor of about 30. At the same time, the response amplitude to NO_2 is decreased while the dynamics are slowed. Results indicate that the addition of Fe deeply modifies both the electrical and gas sensing properties of WO_3. NO_2 is an oxidizing compound and its interaction with n-type metal oxide semiconductors such as WO_3 is usually described by means of a first order reaction between the NO_2 molecule and the oxide surface oxygen vacancies. This leads to the surface oxidation and electrons extraction from the oxide conduction band, thus increasing the material resistance (i.e. $R_{gas} > R_{air}$) as shown in Figure 7. The sensing response performances ($\Delta R/R$, τ_{RESP}, τ_{REC}) of the films to 5 ppm of NO_2 at different temperatures are compared in Table 3. The effect of the sensor temperatures on response parameters is found to be significant on the pure and Fe-doped WO_3 sensors. Increasing the working temperature decreases the response amplitude and decreases the response dynamics. But compared to WO_3, the Fe-doping film shows lower response amplitude and slow response dynamics. At a temperature of 150 °C, the Fe-doping film exhibit a remarkable response ($\Delta R/R$=1100), but with high response and recovery times (τ_{RESP} and τ_{REC} are about 20 minutes). The response parameters of the pure WO_3 sensor heated at 150°C are not reported because the device goes out of range due both to its high baseline resistance (R_{air}=5 GΩ) and its high response. It can only be estimated higher than 4000. In general, the response amplitude of WO_3 based gas sensors is found to be higher at lower temperatures.

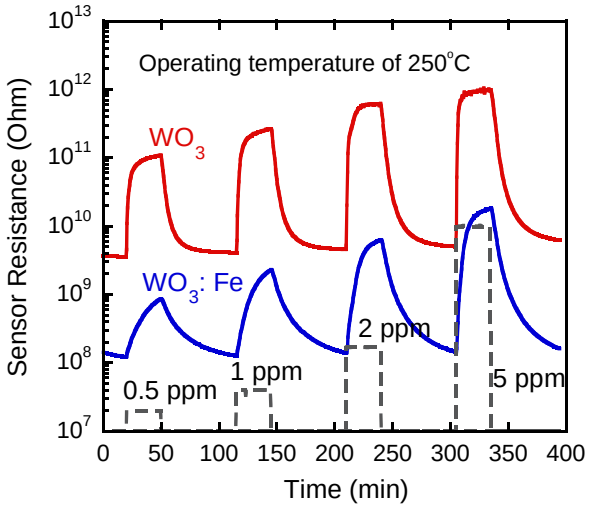

Figure 7 Dynamic response of WO_3 based sensors for different NO_2 concentrations at 200°C, measured in constant flow (300 sccm) and humidity conditions (30% RH at 20°C).

Table 3 Sensor response parameters of e-beam evaporated WO_3 and WO_3:Fe films to 5 ppm NO_2 gas at different temperatures.

	WO_3		WO_3: Fe		
	200°C	250°C	150°C	200°C	250°C
$\Delta R/R$	192	150	1100	130	140
τ_{RESP}	910 s	900 s	1400 s	1360 s	1110 s
τ_{REC}	460 s	250 s	1400 s	675 s	400 s

Sensing Characteristics to NH_3: The sensing response of the pure and Fe-doped WO_3 thin films to 20 ppm ammonia (NH_3) has been measured, as shown in Figure 10. Addition of Fe to the pure film lowers the sensing response to NH_3 gas. Similarly the response of both films decreased with increasing operating temperature of the sesnors, which is the opposite effect observed in NO_2. This result is useful for selectivity purposes, because the specific sensitivity (SS) of the Fe-doped films to NO_2 with respect to NH_3 increases with increasing operating temperature. In this paper a specific selectivity (SS) of the sensors has been determined by dividing the sensitivity value of the selective gas to the corresponding value of a gas to be compared. For example, the response amplitude of the Fe-doped film (400 nm thick) at 250°C to NO_2 (5 ppm) is more than 4000 times higher than the response to NH_3 (20 ppm). For comparison, it is only about 900 times higher in the case of pure WO_3. These specific sensitivity valaues observed in this experiment are much higher than values reported in literature. For example, a ratio lower than 100 has been obtain with WO_3 samples prepred by a modified thermal evaporation method [25] or by ion beam deposition [26].

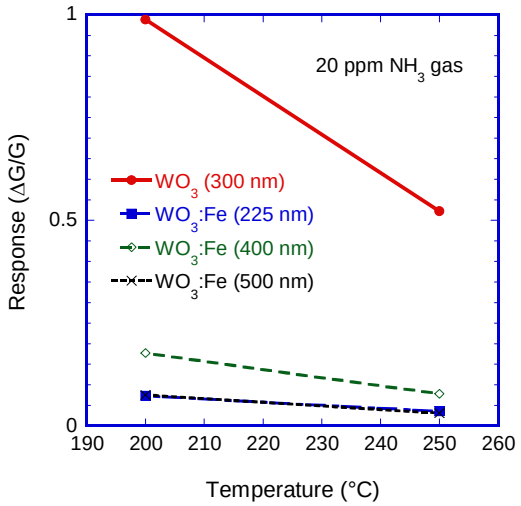

Figure 10 Response amplitude of WO_3 and WO_3:Fe sensors to 20 ppm NH_3 in the operating temperature range of 200-250°C.

Sensing Characteristics to H_2: The dynamic responses of both the e-beam and thermal evaporated films toward a range of concentrations (600-10,000 ppm) of H_2 gas were measured. Figure 11a shows the response amplitude of e-beam evaporated WO_3:Fe film (100 nm thick). From the figure the response amplitude appeared to be much smaller (max. 0.055) than the values obtained to NO_2 and NH_3 gases. Higher response amplitude ($\Delta R/R=10$) is

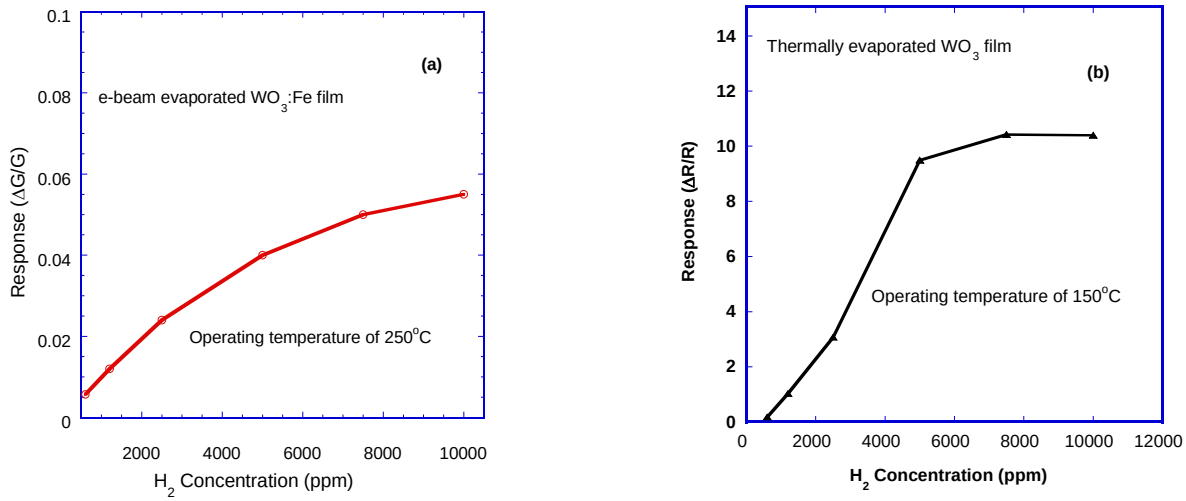

Figure 11 (a) Response amplitude to different H_2 concentrations (600-10,000 ppm). (a) e-beam evaporated WO_3:Fe film, and (b) thermally evaporated WO_3 film. Both are measured in constant flow (200 sccm) and humidity conditions (0% RH at RT).

obtained from the pure WO_3 film deposited by thermal evaporation at a much lower operating temperature of 150°C (Fig. 11b). However, the response and recovery dynamics of this film are very slow (e.g. 140 s and 80 s, respectively for 10,000 ppm). This is not surprising as the gas dynamics slow down at lower operating temperatures.

Sensing Characteristics to CO: There is very little evidence in literature on the sensing of WO_3 thin films to CO gas [27, 28]. In the present study, thermally evaporated pure WO_3 films did not show any response towards CO. However, after Fe-doping and subsequently annealing at 400°C, the film showed a stable and good response to CO at a low operating temperature. Figure 12a shows the response dynamics of the Fe-doped WO_3 film upon exposure to CO of various concentrations (100-1000 ppm). The response increases with increasing CO gas concentration. A response amplitude of $\Delta R/R=0.2$ is obtained at an operating temperature of 150°C (Fig. 12b). The optimum response of the film to CO at a temperature less than 200°C is attributed to a number of factors. The optimum physical, chemical and electrical properties achieved by Fe-doping and annealing of the films strongly influenced their response towards CO at a low operating temperature.

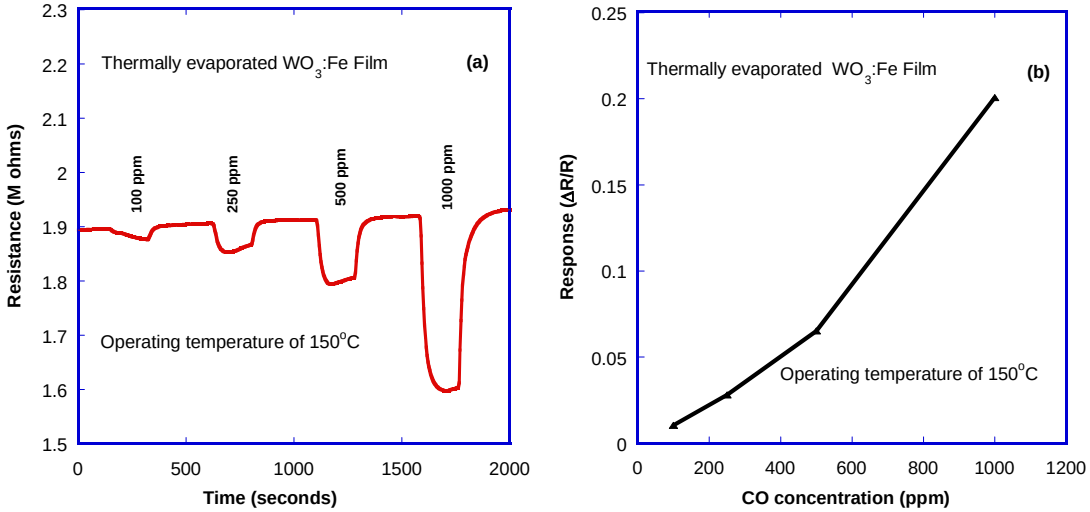

Figure 12 (a) Dynamic response, and (b) response amplitude of thermally evaporated WO_3: Fe films.

Conclusions

The ability to modify the sensing characteristics of WO_3 based oxide sensors is demonstrated by these results. The ability of WO_3 to sense both oxidizing and reducing gases is dependent on achieving a degree of crystallinity, which generally requires some post-deposition heat treatment, especially for the thermally evaporated films. The crystallite size (and films surface area) and porosity of the films dominate the response obtained by the films, while the doping of the WO_3 with Fe generally reduces the response owing to increased grain size in the experiments conducted here, the doping can increase the selectivity of the film for specific gases. In the case of Fe:WO_3, the selectivity of the film to NO_2 is increased relative to the sensitivity to NH_3. An additional benefit of the Fe-doping is an decrease in film resistivity, which makes measuring the response more straightforward, although at the expense of sensitivity.

The as-deposited films were amorphous and annealing of the films above 300^{o}C in air improved the crystallinity and the formation of high porosity and ultrasmall nanoparticles (5-12 nm). The e-beam evaporated films (annealed at 300^{o}C) were found to be amorphous to the XRD but appeared to have some degree of crystallinity from Raman peaks, which is also confirmed by TEM. The thermally evaporated films (annealed at 400^{o}C) show better crystallinity as observed from XRD, Raman and TEM. XPS analysis revealed that the Fe-doped films contain higher number of oxygen vacancies than the pure films, which may explain the increase in selectivity for NO_2 over NH_3. The band gap energy, lattice cell parameters and O-W-O bonding of WO_3 films have been modified by Fe-doping. Addition of 10 at% Fe significantly improved the electrical conductance and making gas sensing measurement easier, especially at lower temperatures, when pure WO_3 exhibits a very high resistance. Experimental results indicated that both the pure and Fe-doped films made by e-beam evaporation achieved excellent sensing response amplitude and selectivity with reasonable response and recover times to NO_2 gas. The specific sensitivity of NO_2 to NH_3 (for example at 250^{o}C) is over 4000 for the Fe-doped WO_3 sensor and only about 900 for the WO_3 sensor. From the results, the effect of doping was found to be more apparent than film thickness effect as observed in both NO_2 and NH_3. The pure films developed by thermal evaporation have shown some response to H_2 whereas the Fe-doped films favored to CO at lower temperature of 150^{o}C. In general, the response amplitudes of both e-beam and thermal evaporated WO_3 based gas sensors are found to be higher at lower temperatures which is highly desirable, especially for remote area field sensing. It is concluded that a combination of the ultra small grain size (<12 nm) and higher porosity obtained through evaporation and subsequent annealing of the films have given excellent sensitivity and selectivity to NO_2 gas.

Acknowledgment

Acknowledgement to Japanese Society for Promotion of Science (JSPS), Queensland Government Smart Futures Fund, and Australian Institute of Nuclear Science and Engineering (AINSE).

References

1. Kunt, T.A., et al., *Optimization of temperature programmed sensing for gas identification using micro-hotplate sensors.* Sensors and Actuators B: Chemical, 1998. **53**(1-2): p. 24-43.

2. Berger, O., et al., *Tungsten-oxide thin films as novel materials with high sensitivity and selectivity to NO2, O3, and H2S. Part II: Application as gas sensors* J. Mater. Sci: Mater. Elect. , 2004. **15**: p. 483-493.
3. Ahsan, M., et al., *Low temperature response of nanostructured tungsten oxide thin films toward hydrogen and ethanol.* Sensors and Actuators B: Chemical, 2012. **173**(0): p. 789-796.
4. Ahsan, M., et al., *Low temperature CO sensitive nanostructured WO3 thin films doped with Fe.* Sensors and Actuators B: Chemical, 2012. **162**(1): p. 14-21.
5. Tesfamichael, T., et al., *Thin Film Deposition and Characterization of Pure and Iron-Doped Electron-Beam Evaporated Tungsten Oxide for Gas Sensors.* Thin Solid Films, 2010. **518** p. 4791–4797.
6. Tesfamichael, T., et al., *Gas sensing characteristics of Fe-doped tungsten oxide thin films.* Sensors and Actuators B: Chemical, 2012. **168**(0): p. 345-353.
7. Wang, X., S.S. Yee, and W.P. Carey, *Transition between neck-controlled and grain-boundary-controlled sensitivity of metal-oxide gas sensors.* Sens. Actuators B Chem, 1995. **25**: p. 454-457.
8. Artzi-Gerlitz, R., et al., *Fabrication and gas sensing performance of parallel assemblies of metal oxide nanotubes supported by porous aluminum oxide membranes.* Sens. Actuators B Chem, 2009. **136**(1): p. 257-264.
9. Kawasaki, H., et al., *Properties of metal doped tungsten oxide thin films for NOx gas sensors grown by PLD method combined with sputtering process.* Sens. Actuators B Chem, 2004. **100**: p. 266-269.
10. Boudiba, A., et al., *Preparation of highly selective, sensitive and stable hydrogen sensors based on Pd-doped tungsten trioxide.* Procedia Engineering, 2010. **5**(0): p. 180-183.
11. Stankova, M., et al., *Sensitivity and selectivity improvement of rf sputtered WO3 microhotplate gas sensors.* Sens. Actuators B Chem, 2006. **113**: p. 241-248.
12. Rossinyol, E., et al., *Mesostructured pure and copper-catalyzed tungsten oxide for NO2 detection.* Sens. Actuators B Chem, 2007. **126**(1): p. 18-23.
13. Comini, E., et al., *Correlation between atomic composition and gas sensing properties in tungsten-iron oxide thin films.* Sens. Actuators B Chem, 2007. **127**: p. 22-28.
14. Roldan, A., et al., *Theoretical Confirmation of the Enhanced Facility to Increase Oxygen Vacancy Concentration in TiO2 by Iron Doping.* The Journal of Physical Chemistry C. **114**(14): p. 6511-6517.
15. Mandayo, G.G., et al., *Strategies to enhance the carbon monoxide sensitivity of tin oxide thin films.* Sens. Actuators B Chem, 2003. **95**: p. 90-96.
16. Berger, O., W.-J. Fischer, and V. Melev, *Tungsten-oxide thin films as novel materials with high sensitivity and selectivity to NO2, O3 and H2S. Part I: Preparation and microstructural characterization of the tungsten-oxide thin films* J. Mater. Sci.: Mater. Elect., 2004. **15**: p. 463-482.
17. Wetchakun, K., et al., *Semiconducting metal oxides as sensors for environmentally hazardous gases.* Sensors and Actuators B: Chemical, 2011. **160**(1): p. 580-591.
18. Sivakumar, R., et al., *Preparation and characterization of electron beam evaporated WO3 thin films.* Opt. Mater., 2007. **29**: p. 679-687.
19. Pal, S. and C. Jacob, *The influence of substrate temperature variation on tungsten oxide thin film growth in an HFCVD system.* Applied Surface Science, 2007. **253**(6): p. 3317-3325.
20. Baserga, A., et al., *Nanostructured tungsten oxide with controlled properties: Synthesis and Raman characterization.* Thin Solid Films, 2007. **515**(16): p. 6465-6469.
21. Jayatissa, A.H., S.-T. Cheng, and T. Gupta, *Annealing effect on the formation of nanocrystals in thermally evaporated tungsten oxide thin films.* Mater Sci Eng B, 2004. **109**: p. 269-275.
22. Bigey, C., L. Hilaire, and G. Maire, *Catalysis on Pd/WO3 and Pd/WO2: Effect of the Modifications of the Surface States Due to Redox Treatments on the Skeletal Rearrangement of Hydrocarbons.* Journal of Catalysis, 1999. **184**: p. 406–420.
23. Katrib, A., et al., *XPS study of MoO2, WO2 and WO3 and their catalytic activities in the izomerization reactions of alkanes.* J. Chim. Phys. , 1997. **94**: p. 1923-1937
24. Penner, S., et al., *The structure and composition of oxidized and reduced tungsten oxide thin films.* Thin Solid Films, 2008. **516**(10): p. 2829-2836.
25. Ponzoni, A., et al., *Nanostructured WO3 deposited by modified thermal evaporation for gas-sensing applications.* Thin Solid Films, 2005. **490**: p. 81-85.
26. Prasad, A.K. and P.I. Gouma, *MoO3 and WO3 based thin film conductimetric sensors for automotive applications.* J. Mater. Sci., 2003. **38**: p. 4347– 4352.
27. Hübner, M., et al., *CO sensing mechanism with WO_3 based gas sensors.* Sensors and Actuators B: Chemical. **151**(1): p. 103-106.
28. Wu, R.J., et al., *The Novel CO sensing material CoOOH-WO_3 with Au and SWCNT performance enhancement.* Sensors and Actuators B: Chemical, 2009. **138**(1): p. 35-41.